

Vibrationally-resolved X-ray spectra of diatomic systems. I. Time-independent simulations with density functional theory

Lu Zhang¹, Minrui Wei¹, Guoyan Ge¹, and Weijie Hua^{*,1}

¹MIIT Key Laboratory of Semiconductor Microstructure and Quantum Sensing, Department of Applied Physics, School of Science, Nanjing University of Science and Technology, 210094 Nanjing, China

* E-mail: wjhua@njjust.edu.cn (W. Hua)

August 1, 2023

Abstract

A systematic first-principles study was conducted on the vibronic fine structures of 5 diatomic systems in their lowest 1s excited (N_2 , N_2^+ , NO^+ , CO , CO^+) or ionized (CO) states, resulting totally 10 X-ray absorption (XAS) or photoelectron (XPS) spectra at the C/N/O K-edges. All calculations were performed within a time-independent (TI) sum-over-states framework under the harmonic oscillator approximation. To assess the performance of different functionals, two common pure (BLYP and BP86) and two hybrid (B3LYP and M06-2X) functionals were employed. Excellent agreement between theoretical and experimental spectra was observed for most systems. However, there were two instances where the peak separations were underestimated in the O1s XAS spectra of CO and NO^+ . This discrepancy was attributed to anharmonic effects. By analyzing rich data on the same footing, we established a connection between the complex fine structures of the two cases to their significant changes in potential energy curves as induced by the core hole. It was found that the functional dependence in diatomic molecules is generally more pronounced compared to polyatomic ones, although the level of sensitivity may vary depending on the specific system and spectroscopy being studied. In all these examples examined, the pure functionals exhibit a better or similar spectral accuracy to the hybrid functionals. This was attributed to superior accuracy in bond lengths and vibrational frequencies (in both the initial and final states) predicted by pure functionals, as compared with the experiments. This study highlights the use of density functional theory with pure functionals for such diatomic calculations due to its easy execution and generally reliable accuracy.

1 Introduction

Spectroscopy links experiment and theory, with precision at the heart. An illustrative example in the history of physics is the hydrogen spectrum, where escalating measurement precision has reciprocally fostered the evolution of quantum theory. High-resolution spectroscopy acts as a litmus test for gauging the precision of theoretical methods used. Particularly, in the context of high-resolution vibrationally-resolved X-ray spectroscopy,[1, 2, 3, 4, 5, 6, 7, 8, 9, 10, 11, 12, 13, 14, 15, 16] comparison to experimental data affords an evaluation of the quality of potential energy surfaces (PESs) for both the core-electron excited (or ionized) and the ground electronic states. It also provides opportunities to scrutinize the accuracy of employed electronic structure methods, especially when dealing with states that encompass a core hole.

Density functional theory (DFT) has emerged as a predominant electronic structure method, offering profound insights into a broad spectrum of molecules and materials. It holds the capability to accurately predict X-ray spectra.[17] The conjunction of DFT with the Duschinsky rotation (DR) method[18] has yielded substantial alignment with experiments for vibrationally-resolved X-ray photoelectron (XPS)[19, 20, 21] and absorption (XAS)[22] spectra, spanning a comprehensive spectrum of molecules, such as benzene,[19] furan,[19] pyridine,[19] azines,[20] polycyclic aromatic hydrocarbons (PAHs),[21] and ions like N_2H^+ . [22] In these calculations, either full core-hole (FCH) or excited core-hole (XCH)[23] approximation was leveraged to describe the core ionized (in the case of XAS) or excited (in the case of XPS) states, while conventional DFT was employed to model the ground state (GS). (In the subsequent context, the term “excited state” is used without distinction to refer to either a core excited or ionized state.) It is worth noting of other DFT applications[8, 24, 19] also with the half core hole (HCH)[25] or the equivalent core hole (ECH, i.e., $Z+1$)[26] approximations. Buoyed by the promising outcomes from DFT computations, we are currently engaged in formulating a theoretical library for vibrationally-resolved XPS/XAS spectra of common molecules and ions, with initial findings already disseminated.[19, 20, 21] Most investigated systems were polyatomic, i.e., composed of three or more atoms.

A diatomic system, with a single vibrational mode, offers a more “transparent” view of vibronic coupling effects and is highly sensitive to the utilized electronic structure method. Diatomic molecules such as N_2 , [27] CO , [28] NO , [28] and ions like NH^+ , [29] N_2^+ , [30] CO^+ , [31] NO^+ , [32] and C_2^- [16] have been extensively investigated through both XPS/XAS experiments[27, 28, 2, 29, 30, 31, 32, 16] and simulations at varied levels.[1, 27, 28, 29, 30, 31, 32, 16] Generally, the results indicate good agreement. Alongside technological advancements in X-ray synchrotron beams for experimental development[11], theoretical methods for X-ray spectra have also seen significant improvements in recent years[1], enabling high-quality theoretical predictions of vibrationally resolved X-ray spectra. Neutral diatomic molecules have been a frequent focus in many X-ray spectral studies due to their ability to reach higher target densities compared to charged particles[16]. Recent innovations in ion beam and ion trap techniques

have facilitated precise inner-shell investigations involving positively charged diatomic molecular ions.[32, 29]

We found that various post-Hartree-Fock methods were used in almost all calculations. Couto et al.[31] presented and analyzed high-resolution XAS spectra of CO^+ , using wavepacket dynamics calculations based on potential energy curves (PECs) computed with the restricted active space second-order perturbation (RASPT2) method. Using the restricted active space multiconfigurational theory self-consistent field (RASSCF) and second-order perturbation (RASPT2) methods, Lindblad et al. interpreted the experimental XAS spectra of N_2^+ [30] and NO^+ . [32] Carniato et al.[29] simulated the PECs of low-lying N1s excited states of NH^+ by using the configuration interaction singles and doubles (CISD) method and the valence-state PECs by multiconfigurational self-consistent field (MCSCF). Rocha[33] simulated PEC of CO in the lowest C1s excited state by the restricted active space SCF (RASSCF) method, termed also as the inner-shell complete active space SCF (IS-CASSCF) method. Martins et al.[34] computed PECs of low-lying F1s core excited states of HF and HF^+ by using the full configuration-interaction method to help understand the photodissociation dynamics. Such studies have been instrumental in enriching our understanding of core-hole state electronic structure, X-ray physics, vibronic coupling, and bond dissociation dynamics. However, such studies typically cover one or only a few systems. Computational studies by different groups frequently take different theoretical levels. There is a lack of simulations of many systems on the same footing, which is essential for enabling fair comparisons and analyses to draw general rules concerning vibronic coupling properties.

The aim of this study is to benchmark the application of DFT in simulating vibrationally-resolved XPS/XAS spectra of diatomic systems. This premise is built upon the ability of DFT to generate accurate potential energy curves (PECs) in close proximity to the Franck-Condon region, despite its potential shortcomings at larger bond distances where multi-configurational effects become pivotal. In this work, the FCH approximation will be deployed for the 1s ionized state and the XCH approximation for the lowest 1s excited state. A variety of common molecules and ions will be used for the XAS (N_2 , N_2^+ , NO^+ , CO , and CO^+) and XPS (CO) spectra, covering the C/N/O K-edges.

Generally, two complementary solutions to vibronic coupling include the time-independent (TI) and time-dependent (TD) frameworks. The TI method is usually based on the harmonic oscillator approximation and mathematically represented by an analytical sum-over-states expression.[35] It involves optimizing the structure of the final state and performing vibrational frequency calculations, which can be challenging for certain systems.[20, 36] However, the spectral interpretations obtained through the TI approach are direct and straightforward. On the other hand, the TD wavepacket method is based on the Fourier transform of the auto-correlation function.[37, 31] This method allows for the inclusion of anharmonic effects that can be included from the input potential energy surfaces. In this study, we specifically present the results obtained using the TI framework. We plan to utilize the TD method in a subsequent study (paper II) [38] in order to get a complete picture.

2 Time-independent method

We use bolded symbols in lower and upper cases for vectors and matrices, respectively, while symbols in normal fonts indicate scalars. The initial (ground) electronic state is denoted by g , and the final (core-excited or core-ionized) electronic state by e . We differentiate any physical quantity in state g or e using a respective symbol with or without a prime. As such, equilibrium geometries (expressed as Cartesian coordinates in column vectors) of the initial and final states are denoted by \mathbf{x}' and \mathbf{x} ; normal coordinates (also in column vectors) for both states are represented by \mathbf{q}' and \mathbf{q} ; respective normal mode matrices are signified by \mathbf{L}' and \mathbf{L} ; vibrational frequencies are designated by ω' and ω ; and bond lengths are represented by R' and R .

The time-independent method was considered based on the harmonic oscillator approximation. Vibrational frequency calculations were first performed at the optimized geometries of both the initial and the final electronic states. The Duschinsky rotation (DR) method[18] was then used to connect both normal coordinates:

$$\mathbf{q}' = \mathbf{J}\mathbf{q} + \mathbf{k}. \quad (1)$$

Here \mathbf{k} indicates the displacement vector between the PESs of both electronic states along the normal coordinate. \mathbf{J} is the Duschinsky rotation matrix, which is 1 for a diatomic system. \mathbf{k} depends on the initial-state normal coordinate matrix \mathbf{L}' , the diagonal matrix of atomic masses \mathbf{M} , and the change between the equilibrium geometries of both states $\Delta\mathbf{x}$ ($\Delta\mathbf{x} \equiv \mathbf{x} - \mathbf{x}'$):

$$\mathbf{k} = (\mathbf{L}')^T \mathbf{M}^{1/2} \Delta\mathbf{x}. \quad (2)$$

The vibrational profile can then be calculated with \mathbf{k} and the vibrational frequencies (ω' and ω).[39, 40, 41]

The 0-0 vibrational transition energy in XAS and XPS spectra are respectively calculated by using the Δ Kohn-Sham (Δ KS) scheme,[42, 43]

$$E_{00}^{\text{XAS}} = E_{\text{XCH}}|_{\text{min XCH}} - E_{\text{GS}}|_{\text{min GS}} + \delta_{\text{rel}}, \quad (3)$$

$$E_{00}^{\text{XPS}} = E_{\text{FCH}}|_{\text{min FCH}} - E_{\text{GS}}|_{\text{min GS}} + \delta_{\text{rel}}, \quad (4)$$

which considers both electronic and geometrical relaxations. Here E_{GS} , E_{FCH} , and E_{XCH} stand for total energies of the ground electronic state, the FCH state with one 1s electron removed, and the XCH state with one 1s electron excited to the lowest unoccupied molecular orbital (LUMO), respectively; **min GS**, **min FCH**, or **min XCH** denotes the optimized structure of each state. δ_{rel} is a small uniform shift considering the differential relativistic effect, which is related to the removal of an electron from the core orbital. The values used for the C, N, and O 1s core holes are $\delta_{\text{rel}} = 0.2, 0.3,$ and 0.4 eV, respectively.[43]

3 Computational details

All electronic structure calculations were carried out at the DFT level by using the GAMESS-US package,[44] enforcing a C_{4v} point group symmetry. Four

different functionals were chosen: BLYP,[46, 47] BP86,[46, 48] B3LYP,[49, 47] and M06-2X.[50] A double basis set technique was used.[19] The aug-cc-pVTZ basis set[51] was used in the geometrical optimization of the ground state. Concerning the excited state, the IGLO-III basis set[53] was set for the excited atom. The basis set for the other atom was chosen as follows: in a homonuclear molecule or ion (N_2 , N_2^+), model core potential (MCP) together with corresponding MCP/TZP basis set[54] was employed; while in a heteronuclear system (CO, CO^+ , NO), the aug-cc-pVTZ basis was set. Unrestricted DFT (UDFT) was employed for all excited-state calculations except for 1s ionized states of CO, where UDFT encountered SCF convergence errors, and restricted open-shell DFT (RO-DFT) was used instead. Vibrational frequency calculations were then performed at the optimized structures (all Cartesian coordinates provided in the Supplementary Material[57]).

Then, a modified DynaVib package [19] was employed to compute the Franck-Condon factors (FCFs) based on the obtained energies, geometries, and vibrational frequencies. The vibrationally-resolved XAS and XPS spectra were obtained by convoluting the stick FCFs with a Lorentzian function. A hwhm value, $\gamma=0.05$ eV, was chosen to achieve better agreement with experimental observations. Here γ is to phenomenologically include many effects for broadening (such as the lifetime, instrumental, and Doppler broadening, and environmental effects) and similar values have been utilized in previous studies for other systems.[19, 20, 36, 21] In principle, one may always use the Voigt convolution (see, e.g., Ref. [22]) to tune a better agreement with the experiment, with the Lorentzian/Gaussian hwhm components read either from a library,[58] or directly from the experiment.[22] Nevertheless, in this work, the hwhm parameter is not a pivotal factor. For simplicity and consistency, a constant hwhm value was utilized in all calculations, which does not impact the validity of our discussions.

4 Results and discussion

4.1 Bond lengths and core-hole induced changes

Table 1 displays the theoretical bond lengths for each system in the optimized ground state (R') and excited state (R), as well as their differences denoted by $\Delta R \equiv R - R'$. A comparison with gas phase experiments is also provided to illustrate the performance of four different functionals. Figure 1 offers a more visual representation of the comparisons. The experimental bond lengths of these systems in the gas phase fall within a narrow range of $R' = 1.063\text{--}1.128$ Å, spanning a difference of 0.065 Å. The 1s core excitation/ionization can lead to both increases (by 0.025–0.163 Å) or decreases (by 0.037–0.065 Å) in bond lengths, depending on the system and the excited atom. This corresponds to positive or negative values of ΔR [as depicted in Fig. 1(b)]. In the excited state, the bond lengths cover a much wider range of 0.228 Å ($R = 1.063\text{--}1.291$ Å).

Our theoretical results obtained from all functionals generally exhibit good

agreement with the experiments [Table 1; Fig. 1(a)]. The mean absolute deviations (MADs) for R (R') predicted by BLYP, BP86, B3LYP, and M06-2X functionals are 0.008, 0.006, 0.008, and 0.014 Å (0.008, 0.008, 0.005, and 0.010 Å), respectively. The maximum absolute deviations (MAXs) are 0.017, 0.017, 0.027, and 0.037 Å (0.010, 0.010, 0.011, and 0.017 Å). The corresponding relative errors for R (R') are 0.2%–1.6%, 0.0%–1.6%, 0.1%–2.3%, and 0.2%–3.4% (0.0%–0.9%, 0.1%–0.9%, 0.2%–1.0%, and 0.5%–1.5%). Regarding ΔR , the deviations from experiments are 0.001–0.008, 0.000–0.007, 0.001–0.020, and 0.001–0.022 Å, respectively. As depicted in Fig. 1, these deviations from experiments are almost imperceptible for R or R' [Fig. 1(a)] and small for ΔR [Fig. 1(b)].

The results show that the pure functionals (BLYP and BP86) generally provide better agreement with the experiments than the two hybrid functionals (B3LYP and M06-2X). Specifically, with the two pure functionals, the best agreement with the experiment[30] is observed in N_2^+ , with absolute deviations of only 0.000-0.002 Å. This is followed by N_2 , which shows absolute deviations of merely 0.000-0.005 Å in comparison to the experiment.[59] The corresponding changes in bond length (ΔR) for N_2^+ and N_2 are found to be 0.038–0.038 and 0.061-0.063 Å, respectively. On the other hand, B3LYP and M06-2X predict the least agreement in terms of ΔR for N_2^+ and N_2 among all examples illustrated in Fig. 1(b)]. Specifically, the deviations by B3LYP are 0.014 and 0.020 Å, while those by M06-2X are 0.021 and 0.022 Å. These findings highlight the superior performance of the pure functionals BLYP and BP86 in accurately predicting the bond lengths.

4.2 Vibrational frequencies and core-hole induced changes

Table 2 presents the vibrational frequencies in the initial (ω') and final (ω) states, along with comparisons to experimental values. The experimental vibrational frequencies span a range of 2169.8–2376.7 cm^{-1} (with a difference of 206.9 cm^{-1}) in the ground state geometry, and a much wider range of 1338.9–2507.6 cm^{-1} (with a difference of 1168.7 cm^{-1}) in the excited state. The values correspond to typical frequencies for stretching vibrational modes. Similarly to the bond lengths, the influence of the core hole on vibrational frequencies does not follow a definite trend, as both frequency increases and decreases are observed.

The deviations between our DFT calculations to experiments appear to be larger for frequencies compared to bond lengths. This is because vibrational frequency corresponds to the second-order energy derivatives of the Cartesian coordinates. The mean absolute deviations for BLYP, BP86, B3LYP, and M06-2X are 38.5, 33.8, 111.7, and 200.7 cm^{-1} for ω (and 44.2, 34.5, 73.3, and 156.0 cm^{-1} for ω'). The maximum deviations are 74.1, 73.0, 315.0, and 475.4 cm^{-1} for ω (and 55.3, 48.8, 122.8, and 210.9 for ω'). The relative deviations for ω (ω') are 0.9%–5.5%, 0.1%–3.7%, 0.4%–13.0%, and 2.3%–20.0% (1.0%–2.6%, 0.6%–2.3%, 1.9%–5.6%, and 4.8%–9.1%). Table 2 also shows the vibrational frequency change in the initial and final states, denoted by $\Delta\omega \equiv \omega - \omega'$. Correspondingly, the deviations are found to be in the range of 3.5–82.0, 2.0–96.2, 11.4–192.2, and 12.5–275.7 cm^{-1} .

The deviations for ω' or ω are small for the pure functionals and acceptable for the hybrid functionals, as shown in Fig. 1(c). In terms of $\Delta\omega$, the deviations by BLYP or BP86 are small, while the results by B3LYP or M06-2X are acceptable for most examples, as displayed in Fig. 1(d). The largest deviation occurs in N_2^+ , with a value of 192.2 cm^{-1} by B3LYP and 275.7 cm^{-1} by M06-2X, respectively.

The analysis of vibrational frequencies supports the same conclusion as the bond lengths, namely that the pure functionals yield better results compared to the hybrid functionals. Our DFT calculations demonstrate reasonable accuracy in predicting vibrational frequencies, considering the absolute values of experimental frequencies are some $2100\text{-}2400 \text{ cm}^{-1}$ in the ground state and $1300\text{-}2500 \text{ cm}^{-1}$ in the excited state. Moreover, our calculations show balanced accuracy in both the ground and excited states, as indicated by the similar MAD values for the same functional. Similar levels of accuracy have been reported in other studies. For instance, Moitra et al.[60] achieved an overestimation of 90 cm^{-1} (2233 cm^{-1} predicted *versus* 2143 cm^{-1} experimental) and 102 cm^{-1} (2432 cm^{-1} predicted *versus* 2330 cm^{-1} experimental) for CO and N_2 , respectively, in the ground state by using the MP2 method.

4.3 XAS of N_2 and N_2^+

Figures 2-5 illustrate the simulated vibrationally-resolved XAS spectra of N_2 , N_2^+ , NO^+ , CO, and CO^+ computed using DFT with four different functionals. It is generally observed that functional dependence is more pronounced in diatomic molecules compared to polyatomic ones. For instance, weak functional dependence was observed in the vibrationally-resolved N1s XPS spectrum of pyrimidine ($\text{C}_4\text{H}_4\text{N}_2$).[20] However, for diatomic systems, noticeable differences can often be observed in the spectra computed by the four functionals. The level of sensitivity may vary depending on the specific system and spectroscopy being studied. It is interesting to note that the functional sensitivity appears to be diminished in polyatomic systems due to the presence of multiple vibrational modes. In such cases, the combined effects of various vibrational modes tend to wash out the functional dependence. Nonetheless, in most case studies, theoretical results demonstrate good agreement with experimental observations.

Figure 2 presents our computed N1s XAS spectra of N_2 and N_2^+ compared with the experiments.[6, 61, 30] In Fig. 2(a), the experimental spectrum exhibits five distinct vibronic features, with the 0-0 and 0-1 peaks having nearly equal intensities. Our BLYP and BP86 calculations accurately predict the peak separations (corresponding to the vibrational frequencies) and relative peak intensities. In a diatomic system, the peak separation is equivalent to the vibrational frequency, and the agreement in separation here is consistent with the discussion in Section 4.2 (also refer to Table 2). BLYP yields almost identical intensities for the 0-0 and 0-1 peaks, showing the best agreement with the experiment. BP86 shows a slightly weaker 0-1 peak than the 0-0 peak. On the other hand, B3LYP and M06-2X predicted relatively large peak separations and the 0-1 peak intensity is approximately two-thirds of the 0-0 peak. Overall, our

results suggest that pure functionals perform better than hybrid functionals in this case.

In Fig. 2(b), the 0-0 experiment peak of N_2^+ (394.29 eV) experiences a redshift of 7.20 eV compared to N_2 (401.49 eV), which is consistent with valence shell ionization. Additionally, three vibronic features are evident in the experimental spectrum, with the 0-1 peak having approximately half the intensity of the 0-0 peak. Similarly, BLYP and BP86 predict peak separations in good agreement with the experiment and reproduce the relative peak intensities with a slight underestimation of the 0-1 peak intensities. On the other hand, B3LYP and M06-2X slightly overestimate the peak separations and the 0-1 peak intensity compared to the 0-0 peak. They exhibit a slower decay in intensity with respect to the increasing vibrational quantum number n , compared to the experimental trend.

4.4 XAS of NO^+

Figure 3 displays the XAS results of NO^+ at both the N1s and O1s edges. In the N1s edge (panel a), all four functionals show good agreement with the experimental spectrum,[32] which exhibits five distinct vibronic features with approximately equal intensities for the 0-0 and 0-1 peaks. The pure functionals accurately predict the peak separations, although they slightly underestimate the intensity of the 0-1 peak and exhibit a faster decay with increasing vibrational quantum number n . On the other hand, the hybrid functionals (B3LYP and M06-2X) slightly overestimate the peak separations but match the experiment well in terms of peak intensities, with the 0-0 and 0-1 peaks having similar intensities.

In the O1s edge (panel b), the experiment spectrum[32] displays more complex structures with ten relatively weak vibronic features. To some extent, it seems challenging to accurately identify the 0-0 peak. All four functionals yield similar theoretical spectra that show only acceptable agreement with the experiment. While the general shapes of the peak profiles are consistent, the theory underestimates the peak separations.

The discrepancy between the theoretical and experimental XAS spectra in the O1s edge of NO^+ can be attributed to the harmonic oscillator approximation used. In this case, a better agreement with the experiment was achieved by considering anharmonic effects through the use of RASPT2 potential energy curves.[22] The underlying electronic structure reason lies in the fact that O1s core excitation in NO^+ induces a large change in the potential energy surface, including shifts in equilibrium position and alterations in curvature. As mentioned above, the O1s core excitation in NO^+ led to a bond length increase of +0.140 Å (from 1.063 to 1.203 Å) and a decrease in vibrational frequency of -841.8 cm^{-1} (from 2376.7 to 1534.9 cm^{-1}). These changes represent the second largest (Table 1) and the largest (Table 2) among all the examples studied. Additionally, we think the anharmonic effect can be decomposed into two parts: one originating from the vibronic coupling method and the other from the electronic structure method. It would be interesting to separate these two parts

through wavepacket simulations based on PECs generated by DFT. This topic will be covered in a subsequent study.[38]

4.5 XAS of CO and CO⁺

Figure 4 shows the XAS spectra of CO in both the C1s and O1s edges. CO and NO⁺ are isoelectronic species. The results of CO show very similar performance to NO⁺. In the C1s edge (panel a), the experimental spectrum exhibited only two simple features, while the O1s edge (panel b) displayed approximately 12 weak features within a broad peak. All functionals produced spectra with weak functional dependence. They all predict good agreement to the experiment in the C1s edge and acceptable agreement in the O1s edge. In the O1s edge, all theories underestimated the peak separations, similar to the case of NO⁺ in the O1s edge. The underlying structural reason is also the significant changes in the PEC as induced by O1s core excitation. Specifically, the bond length increased by +0.163 Å (from 1.128 to 1.291 Å) and the vibrational frequency decreased by -830.9 cm⁻¹ (from 2169.8 to 1338.9 cm⁻¹). These changes represent the largest (Table 1) and the second-largest (Table 2) among all examples studied.

The case of CO⁺ is much simpler. Figure 5 displays the XAS spectra of CO⁺ in both the C1s and O1s edges. The valence-shell ionization from CO to CO⁺ resulted in a red shift of the experimental 0-0 peak in both edges: -5.25 eV (from 287.29 to 282.04 eV) in the C1s edge and -5.20 eV (from 533.62 to 528.42 eV) in the O1s edge. In both edges, all four functionals achieved good agreement with the experiment[31] in terms of energies and profiles, exhibiting only weak functional dependence.

4.6 XPS of CO

All examples above are on XAS spectra. Shifting our focus to XPS spectra, Fig. 6 presents the simulated vibrationally-resolved XPS spectra of CO at the C and O 1s edges. In comparison to the XAS experiments, the 0-0 peak in both edges exhibits blue shifts: +8.84 eV (from 287.29 to 296.13 eV) and +9.00 eV (from 533.62 to 542.62 eV). The experimental XPS spectra[2] show simple vibronic features at both edges, and all four functionals accurately reproduced the experimental spectra. However, it should be noted that the hybrid functional M06-2X slightly overestimated the intensity of the 0-1 peak in the C1s edge [Fig. 6(a)].

By comparing the XAS [Fig. 4(b)] and XPS [Fig. 6(b)] spectra of CO at the O1s edge, one can find the different responses of the final-state PES induced by O1s excitation and ionization. This may be related to the odd or even number of electrons.

5 Summary and Conclusions

To summarize, within the time-independent framework and the harmonic oscillator approximation, we have systematically assessed the vibrationally-resolved XAS (N_2 , N_2^+ , NO^+ , CO , CO^+) and XPS (CO) spectra of a series of diatomic systems by DFT with four different functionals. In most cases, the theoretical spectra matched well with the experiments. Two exceptions were observed for the O1s XAS of NO^+ and CO , where the theory predicted similar but compressed profiles (i.e., underestimation of peak separations) due to strong anharmonic effects. Comparisons with experiments show good agreement, with the pure functionals (BLYP and BP86) generally performing better or similarly to the two hybrid functionals (B3LYP and M06-2X). The sensitivity of different functional depends on systems, with evident dependence observed in XAS spectra of N_2 , N_2^+ , and NO^+ , while weak dependence was found in the remaining cases.

This study provides a systematic assessment of the DFT method for simulating vibrationally-resolved XAS/XPS spectra of common diatomic systems in the TI framework with the harmonic oscillator approximation. Within this framework, we are able to directly analyze the changes in geometries and vibrational frequencies to examine the core hole effect. With calculations on the same foot for multiple systems, we are able to correlate the spectral fine structures to the underlying geometrical and electronic structure changes. For instance, the large change in PECs leads to complex, multiple weak features in the broad peak. Further analysis of anharmonic effects in the time-dependent framework will be conducted in subsequent studies.[38]

Acknowledgments

This work was inspired by a previous collaborative study on NO^+ , and we thank Dr. Rebecka Lindblad for sending us the raw experimental XAS spectra of NO^+ and Prof. Hans Ågren and Dr. Rafael Couto for helpful discussions. Financial support from the National Natural Science Foundation of China (Grant No. 12274229) and the Postgraduate Research & Practice Innovation Program of Jiangsu Province (Grant Nos. KYCX22_0425 and KYCX22_0424) is greatly acknowledged.

References and Notes

References

- [1] Carravetta V, Couto R C and Ågren H 2022 *J. Phys.: Condens. Matter* **34** 363002

- [2] Hergenbahn U 2004 *J. Phys. B: At. Mol. Opt. Phys.* **37** R89–R135 and Fig. 5 therein, with the experimental C1s and O1s XPS spectra of CO, has been recaptured in our Fig. 6.
- [3] Svensson S 2005 *J. Phys. B: At. Mol. Opt. Phys.* **38** S821–S838
- [4] Siegbahn K 1969 *ESCA applied to free molecules* (North-Holland Publishing)
- [5] Gel’Mukhanov F, Mazalov L and Kondratenko A 1977 *Chem. Phys. Lett.* **46** 133–137
- [6] Chen C T, Ma Y and Sette F 1989 *Phys. Rev. A* **40** 6737–6740 ISSN 0556-2791 and Fig. 2(a) therein, with the experimental N1s XAS spectrum of N₂, has been recaptured in our Fig. 2(a).
- [7] Rennie E, Kemppens B, Köppe H, Hergenbahn U, Feldhaus J, Itchkawitz B, Kilcoyne A, Kivimäki A, Maier K, Piancastelli M and others 2000 *J. Chem. Phys.* **113** 7362–7375
- [8] Minkov I, Gel’Mukhanov F, Friedlein R, Osikowicz W, Suess C, Öhrwall G, Sorensen S L, Braun S, Murdey R, Salaneck W R and Ågren H 2004 *J. Chem. Phys.* **121** 5733–5739
- [9] Hoshino M, Montuoro R, Lucchese R R, De Fanis A, Hergenbahn U, Prümper G, Tanaka T, Tanaka H and Ueda K 2008 *J. Phys. B: At. Mol. Opt. Phys.* **41** 085105 ISSN 0953-4075, 1361-6455 URL <https://iopscience.iop.org/article/10.1088/0953-4075/41/8/085105>
- [10] Fronzoni G, Baseggio O, Stener M, Hua W, Tian G, Luo Y, Apicella B, Alfé M, de Simone M, Kivimäki A and Coreno M 2014 *J. Chem. Phys.* **141** 044313
- [11] Mosnier J P, Kennedy E T, van Kampen P, Cubaynes D, Guilbaud S, Sisourat N, Puglisi A, Carniato S and Bizau J M 2016 *Phys. Rev. A* **93** 061401(R)
- [12] Vaz da Cruz V, Ertan E, Ignatova N, Couto R C, Polyutov S, Odelius M, Kimberg V and Gel’Mukhanov F 2018 *Phys. Rev. A* **98** 012507
- [13] Michelitsch G S and Reuter K 2019 *J. Chem. Phys.* **150** 074104
- [14] Kjellsson L 2021 *X-ray spectroscopy on diatomic and cationic molecules* Ph.D. thesis Uppsala University
- [15] Huang M, Li C and Evangelista F A 2022 *J. Chem. Theory Comput.* **18** 219–233 ISSN 1549-9618, 1549-9626
- [16] Schippers S, Hillenbrand P M, Perry-Sassmannshausen A, Buhr T, Fuchs S, Reinwardt S, Trinter F, Müller A and Martins M 2023 *ChemPhysChem* ISSN 1439-4235, 1439-7641

- [17] Besley N A 2020 *Acc. Chem. Res.* **53** 1306–1315 ISSN 0001-4842, 1520-4898
- [18] Duschinsky F 1937 *Acta Physicochim. URSS* **7**
- [19] Hua W, Tian G and Luo Y 2020 *Phys. Chem. Chem. Phys.* **22** 20014–20026 ISSN 1463-9076, 1463-9084
- [20] Wei M, Cheng X, Zhang L, Zhang J R, Wang S Y, Ge G, Tian G and Hua W 2022 *Phys. Rev. A* **106** 022811 ISSN 2469-9926, 2469-9934
- [21] Cheng X, Wei M, Tian G, Luo Y and Hua W 2022 *J. Phys. Chem. A* **126** 5582–5593 ISSN 1089-5639, 1520-5215
- [22] Couto R C, Hua W, Lindblad R, Kjellsson L, Sorensen S L, Kubin M, Bülow C, Timm M, Zamudio-Bayer V, Von Issendorff B, Söderström J, Lau J T, Rubensson J E, Ågren H and Carravetta V 2021 *Phys. Chem. Chem. Phys.* **23** 17166–17176 ISSN 1463-9076, 1463-9084
- [23] Prendergast D and Galli G 2006 *Phys. Rev. Lett.* **96** 215502 ISSN 0031-9007, 1079-7114
- [24] Minkov I, Gelmukhanov F, Ågren H, Friedlein R, Suess C and Salaneck W R 2005 *J. Phys. Chem. A* **109** 1330–1336
- [25] Triguero L, Pettersson L G M and Ågren H 1998 *Phys. Rev. B* **58** 8097–8110
- [26] Jolly W L and Hendrickson D N 1970 *J. Am. Chem. Soc.* **92** 1863–1871
- [27] Ehara M, Nakatsuji H, Matsumoto M, Hatamoto T, Liu X J, Lischke T, Prümper G, Tanaka T, Makochekanwa C, Hoshino M, Tanaka H, Harries J R, Tamenori Y and Ueda K 2006 *J. Chem. Phys.* **124** 124311 ISSN 0021-9606, 1089-7690
- [28] Püttner R, Dominguez I, Morgan T J, Cisneros C, Fink R F, Rotenberg E, Warwick T, Domke M, Kaindl G and Schlachter A S 1999 *Phys. Rev. A* **59** 3415–3423 ISSN 1050-2947, 1094-1622 and Fig. 1 therein, with the experimental O1s XAS spectrum of CO, has been recaptured in our Fig. 4(b)
- [29] Carniato S, Bizau J M, Cubaynes D, Kennedy E T, Guilbaud S, Sokell E, McLaughlin B and Mosnier J P 2020 *Atoms* **8** 67 ISSN 2218-2004
- [30] Lindblad R, Kjellsson L, Couto R C, Timm M, Bülow C, Zamudio-Bayer V, Lundberg M, von Issendorff B, Lau J T, Sorensen S L, Carravetta V, Ågren H and Rubensson J E 2020 *Phys. Rev. Lett.* **124** 203001 ISSN 0031-9007, 1079-7114 and Fig. 2 therein, with the experimental N1s XAS spectra of N_2^+ , has been recaptured in our Fig. 2(b).

- [31] Couto R C, Kjellsson L, Ågren H, Carravetta V, Sorensen S L, Kubin M, Bülow C, Timm M, Zamudio-Bayer V, von Issendorff B, Lau J T, Söderström J, Rubensson J E and Lindblad R 2020 *Phys. Chem. Chem. Phys.* **22** 16215–16223 and Fig. 2(a) therein, with the experimental C1s and O1s XAS spectra of CO⁺, has been recaptured in our Fig. 5.
- [32] Lindblad R, Kjellsson L, De Santis E, Zamudio-Bayer V, von Issendorff B, Sorensen S L, Lau J T, Hua W, Carravetta V, Rubensson J E, Ågren H and Couto R C 2022 *Phys. Rev. A* **106** 042814 ISSN 2469-9926, 2469-9934 and Fig. 3 therein, with the experimental N1s and O1s XAS spectra of NO⁺, has been recaptured in our Fig. 3.
- [33] Rocha A B 2011 *J. Chem. Phys.* **134** 024107
- [34] Martins M, Reinwardt S, Schunck J O, Schwarz J, Baev K, Müller A, Buhr T, Perry-Sassmannshausen A, Klumpp S and Schippers S 2021 *J. Phys. Chem. Lett.* **12** 1390–1395
- [35] Cerezo J and Santoro F 2023 *J. Comput. Chem.* **44** 626–643 ISSN 0192-8651, 1096-987X
- [36] Wei M, Zhang L, Tian G and Hua W 2023 Vibronic fine structure in the nitrogen 1s photoelectron spectra from Franck-Condon simulations II: Indoles arXiv:2307.01510 [physics]
- [37] Gel'mukhanov F and Ågren H 1999 *Phys. Rep.* **312** 87–330 ISSN 03701573
- [38] Zhang L, Ge G, Wei M and Hua W Vibrationally-resolved x-ray spectra of diatomic systems. II. Time-dependent wavepacket simulations to be submitted
- [39] Sharp T and Rosenstock H 1964 *J. Chem. Phys.* **41** 3453–3463
- [40] Ruhoff P T 1994 *Chem. Phys.* **186** 355–374
- [41] Ruhoff P T and Ratner M A 2000 *Int. J. Quantum Chem.* **77** 383–392
- [42] Bagus P S 1965 *Phys. Rev.* **139**(3A) A619–A634
- [43] Triguero L, Plashkevych O, Pettersson L and Ågren H 1999 *J. Electron. Spectrosc. Relat. Phenom.* **104** 195–207 ISSN 03682048
- [44] Gordon M S and Schmidt M W 2005 Advances in electronic structure theory *Theory and Applications of Computational Chemistry* (Elsevier) pp 1167–1189 ISBN 978-0-444-51719-7
- [45] Schmidt M W, Baldrige K K, Boatz J A, Elbert S T, Gordon M S, Jensen J H, Koseki S, Matsunaga N, Nguyen K A, Su S, Windus T L, Dupuis M and Montgomery J A 1993 *J. Comput. Chem.* **14** 1347–1363 ISSN 0192-8651, 1096-987X

- [46] Becke A D 1988 *Phys. Rev. A* **38** 3098–3100 ISSN 0556-2791
- [47] Lee C, Yang W and Parr R G 1988 *Phys. Rev. B* **37** 785–789 ISSN 0163-1829
- [48] Perdew J P 1986 *Phys. Rev. B* **33** 8822–8824 ISSN 0163-1829
- [49] Becke A D 1993 *J. Chem. Phys.* **98** 5648–5652 ISSN 0021-9606, 1089-7690
- [50] Zhao Y and Truhlar D G 2008 *Theor. Chem. Acc.* **119** 525–525 ISSN 1432-881X, 1432-2234
- [51] Dunning T H 1989 *J. Chem. Phys.* **90** 1007–1023 ISSN 0021-9606, 1089-7690
- [52] Kendall R A, Dunning T H and Harrison R J 1992 *J. Chem. Phys.* **96** 6796–6806 ISSN 0021-9606, 1089-7690
- [53] Kutzelnigg W, Fleischer U and Schindler M 1990 The IGLO-Method: Ab-initio Calculation and Interpretation of NMR Chemical Shifts and Magnetic Susceptibilities *Deuterium and Shift Calculation* vol 23 ed Diehl P, Fluck E, Günther H, Kosfeld R and Seelig J (Berlin, Heidelberg: Springer Berlin Heidelberg) pp 165–262 ISBN 978-3-642-75934-5 978-3-642-75932-1 series Title: NMR Basic Principles and Progress
- [54] Sakai Y, Miyoshi E, Klobukowski M and Huzinaga S 1997 *J. Chem. Phys.* **106** 8084–8092
- [55] Noro T, Sekiya M and Koga T 1997 *Theor. Chem. Acc.* **98** 25–32
- [56] Segmented Gaussian Basis Set. <http://sapporo.center.ims.ac.jp/sapporo/>. Accessed on 2023-7-4.
- [57] See Supplemental Material at [URL will be inserted by publisher] for optimized Cartesian coordinates of all diatomic systems
- [58] Zschornack G H 2007 *Handbook of X-Ray Data* (New York: Springer)
- [59] Neeb M, Rubensson J E, Biermann M and Eberhardt W 1994 *J. Electron. Spectrosc. Relat. Phenom.* **67** 261–274 ISSN 03682048
- [60] Moitra T, Madsen D, Christiansen O and Coriani S 2020 *J. Chem. Phys.* **153** 234111 ISSN 0021-9606, 1089-7690
- [61] Hitchcock A and Brion C 1980 *J. Electron. Spectrosc. Relat. Phenom.* **18** 1–21 ISSN 03682048 and Fig. 5 therein, with the experimental N1s XAS spectrum of N₂, has been recaptured in our Fig. 2(a), and Fig. 6(a) therein, with the experimental C1s XAS spectrum of CO, has been recaptured in our Fig. 4(a).
- [62] Albritton D L, Schmeltekopf A L and Zare R N 1979 *J. Chem. Phys.* **71** 3271–3279 ISSN 0021-9606, 1089-7690

[63] Laher R R and Gilmore F R 1991 *J. Phys. Chem. Ref. Data* **20** 685–712
ISSN 0047-2689, 1529-7845

Table 1: Comparison of bond lengths (in Å) in the optimized ground (R') and 1s excited/ionized (R) states of selected diatomic systems by the DFT method with different functionals.

Compound	Expt.			BLYP			BP86			B3LYP			M06-2X		
	R'	R	ΔR^a	R'	R	ΔR	R'	R	ΔR	R'	R	ΔR	R'	R	ΔR
N ₂	1.098 ^{e, f}	1.164 ^{f, i}	+0.066	1.103	1.167	+0.063	1.103	1.164	+0.061	1.092	1.137	+0.046	1.087	1.130	+0.044
N ₂ ⁺	1.116 ^f	1.076	-0.040 ^j	1.116	1.078	-0.038	1.115	1.078	-0.038	1.105	1.051	-0.054	1.099	1.039	-0.061
NO ⁺ (N) ^b	1.063 ^g	1.123	+0.060 ^k	1.072	1.129	+0.058	1.071	1.125	+0.055	1.057	1.117	+0.059	1.050	1.109	+0.059
NO ⁺ (O)	1.063	1.203	+0.140 ^k	1.072	1.211	+0.139	1.071	1.205	+0.134	1.057	1.199	+0.141	1.050	1.193	+0.142
CO(C)	1.128 ^{f, h}	1.153 ^f	+0.025	1.138	1.164	+0.026	1.138	1.161	+0.023	1.126	1.156	+0.029	1.122	1.155	+0.034
CO(O)	1.128	1.291 ^h	+0.163	1.138	1.300	+0.162	1.138	1.295	+0.157	1.126	1.292	+0.165	1.122	1.293	+0.172
CO ⁺ (C)	1.115 ^f	1.078	-0.037 ^l	1.125	1.080	-0.045	1.124	1.080	-0.044	1.110	1.068	-0.043	1.102	1.059	-0.044
CO ⁺ (O)	1.115	1.162	+0.047 ^l	1.125	1.176	+0.051	1.124	1.175	+0.051	1.110	1.163	+0.052	1.102	1.156	+0.054
CO(C)[XPS] ^c	1.128	1.063	-0.065 ^m	1.138	1.080	-0.058	1.138	1.080	-0.059	1.126	1.068	-0.059	1.122	1.059	-0.063
CO(O)[XPS]	1.128	1.165	+0.037 ^m	1.138	1.176	+0.038	1.138	1.175	+0.037	1.126	1.163	+0.036	1.122	1.156	+0.035
MAD ^d	-	-	-	0.008	0.008	0.003	0.008	0.006	0.004	0.005	0.008	0.006	0.010	0.014	0.008
MAX ^d	-	-	-	0.010	0.017	0.008	0.010	0.017	0.007	0.011	0.027	0.020	0.017	0.037	0.022

^a $\Delta R \equiv R - R'$, changes of bond length in Å.

^b For compound with two different elements, the core excitation/ionization center is specified in parenthesis.

^c [XPS] denotes comparison of initial and final states involved in XPS. The rest are for XAS.

^d MAD, mean absolute derivation; MAX, maximum absolute deviation.

^e Ehara et al.[27]

^f Neeb et al.[59]

^g Albritton et al.[62]

^h Püttner et al.[28]

ⁱ Chen et al.[6]

^j Lindblad et al.[30]

^k Lindblad et al.[32]

^l Couto et al.[31]

^m Hergenhahn.[2]

Table 2: Comparison of vibrational frequencies (in cm^{-1}) in the optimized ground (ω') and 1s excited/ionized (ω) states of selected diatomic systems by the DFT method with different functionals.

Compound	Expt.			BLYP			BP86			B3LYP			M06-2X		
	ω'	ω	$\Delta\omega^a$	ω'	ω	$\Delta\omega$	ω'	ω	$\Delta\omega$	ω'	ω	$\Delta\omega$	ω'	ω	$\Delta\omega$
N_2	2359.0 ^e	[†] 1966.2 [†]	-392.8	2334.9	1938.0	-396.9	2345.7	1963.5	-382.2	2449.1	2175.3	-273.8	2522.6	2255.9	-266.7
N_2^+	2207.4 ^f	[‡] 2420.8 [‡]	+213.4	2234.1	2442.3	+208.1	2253.3	2456.8	+203.5	2330.2	2735.8	+405.6	2407.2	2896.2	+489.1
$\text{NO}^+(\text{N})^b$	2376.7 ^h	1954.3 ^j	-422.4	2333.3	1987.8	-345.6	2353.6	2027.3	-326.2	2479.1	2077.5	-401.6	2587.6	2226.7	-360.9
$\text{NO}^+(\text{O})$	2376.7	1534.9 ^j	-841.8	2333.3	1512.6	-820.8	2353.6	1553.1	-800.5	2479.1	1584.1	-895.0	2587.6	1647.4	-940.2
$\text{CO}(\text{C})$	2169.8 ^f	ⁱ 2083.6 ^f	-86.2	2114.5	2015.8	-98.8	2121.0	2042.6	-78.4	2210.9	2091.3	-119.7	2273.9	2130.4	-143.5
$\text{CO}(\text{O})$	2169.8	1338.9 ⁱ	-830.9	2114.5	1264.8	-849.7	2121.0	1292.1	-828.9	2210.9	1302.0	-908.9	2273.9	1304.0	-969.9
$\text{CO}^+(\text{C})$	2214.2 ^f	2507.6 ^k	+293.4	2172.5	2478.6	+306.1	2192.0 ^m	2490.0	+298.0	2289.8	2612.5	+322.7	2393.3	2748.2	+354.9
$\text{CO}^+(\text{O})$	2214.2	1817.2 ^k	-397.0	2172.5	1779.0	-393.5	2192.0	1787.9	-404.1	2289.8	1875.3	-414.6	2393.3	1939.3	-454.0
$\text{CO}(\text{C})[\text{XPS}]^c$	2169.8	2451.9 ^l	+282.1	2114.5	2478.6	+364.1	2121.0	2490.0	+368.9	2210.9	2612.5	+401.6	2273.9	2748.2	+474.4
$\text{CO}(\text{O})[\text{XPS}]$	2169.8	1822.8 ^l	-347.0	2114.5	1779.0	-335.5	2121.0	1787.9	-333.1	2210.9	1875.3	-335.6	2273.9	1939.3	-334.5
MAD ^d	-	-	-	44.2	38.5	24.8	34.5	33.8	28.0	73.3	111.7	67.5	156.0	200.7	108.1
MAX ^d	-	-	-	55.3	74.1	82.0	48.8	73.0	96.2	122.8	315.0	192.2	210.9	475.4	275.7

^a $\Delta\omega \equiv \omega - \omega'$, changes of frequency in cm^{-1} .

^b For the compound with two different elements, the core excitation/ionization center is specified in parenthesis.

^c [XPS] denotes comparison of initial and final states involved in XPS. The rest are for XAS.

^d MAD, mean absolute derivation; MAX, maximum absolute deviation.

^e Ehara et al.[27]

^f Neeb et al.[59]

^g Laher et al.[63]

^h Albritton et al.[62]

ⁱ Püttner et al.[28]

^j Lindblad et al.[32]

^k Couto et al.[31]

^l Hergenbahn.[2]

^m By restricted open-shell DFT (RO-DFT; the rest are by unrestricted DFT).

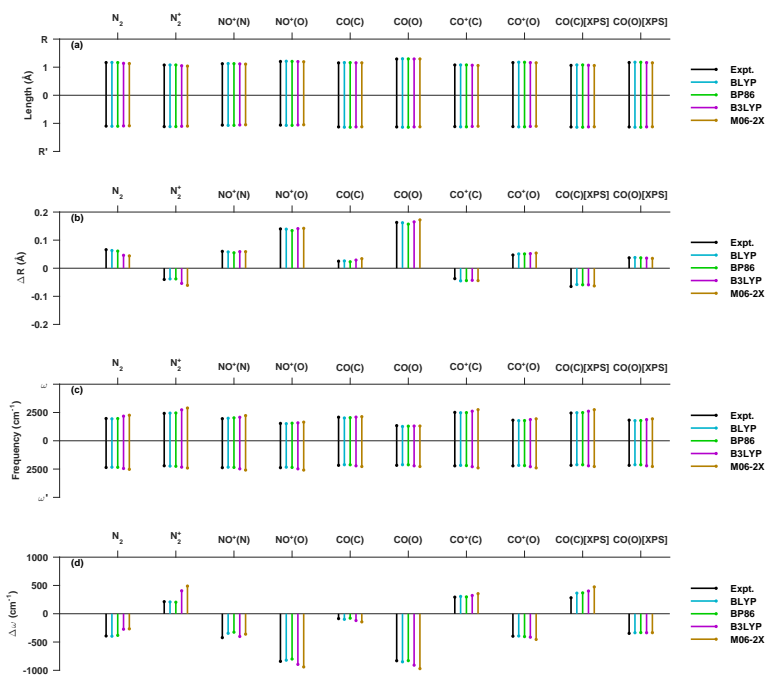


Figure 1: Comparison of parameters in the DFT-optimized structures for the ground and 1s excited/ionized states of diatomic systems with various functionals: (a) Bond lengths in the ground state (R') and excited state (R), (b) changes in bond length (ΔR), (c) vibrational frequencies in the ground state (ω') and excited state (ω), and (d) changes in frequency ($\Delta\omega$). The experimental data used for comparison are the same as those presented in Tables 1 and 2.

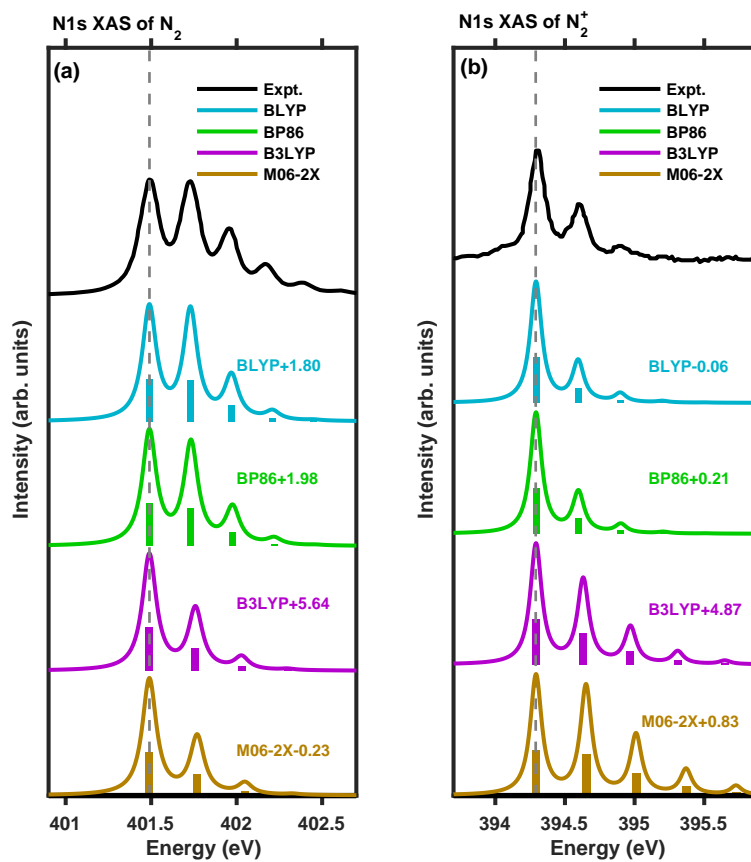


Figure 2: Vibrationally-resolved N1s XAS spectra for (a) N₂ and (b) N₂⁺ simulated with different DFT functionals in the time-independent framework. To better compare with the experiments,[6, 61, 30] theoretical spectra have been shifted (indicated by numbers in eV) by aligning the first peak.

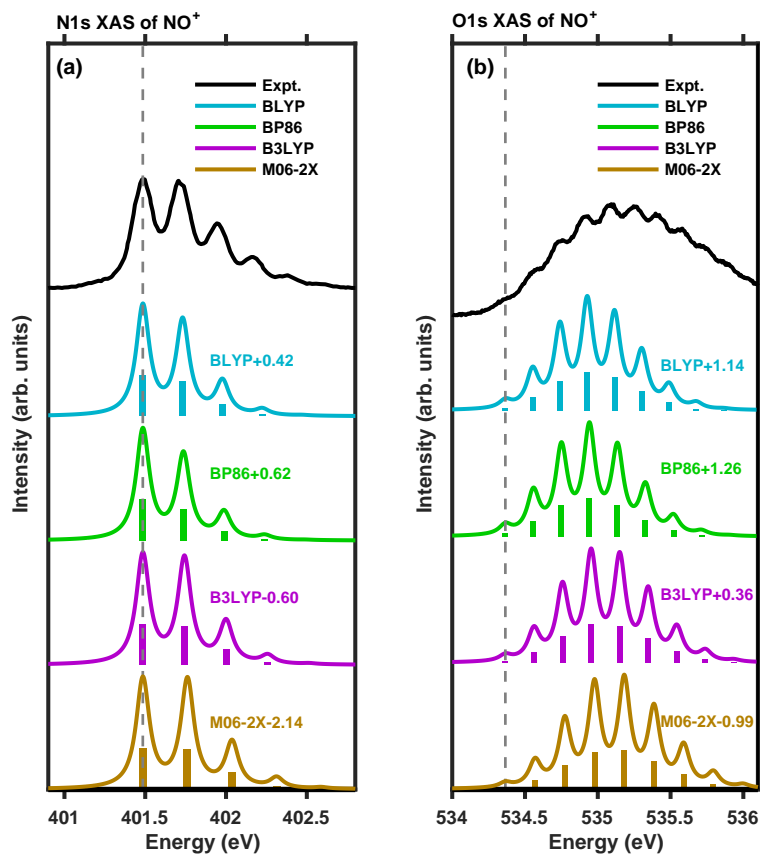


Figure 3: Vibrationally-resolved XAS spectra for NO^+ simulated with different DFT functionals in the time-independent framework: (a) N1s and (b) O1s edges. To better compare with the experiment,[32] theoretical spectra have been shifted (indicated by numbers in eV) by aligning the first peak.

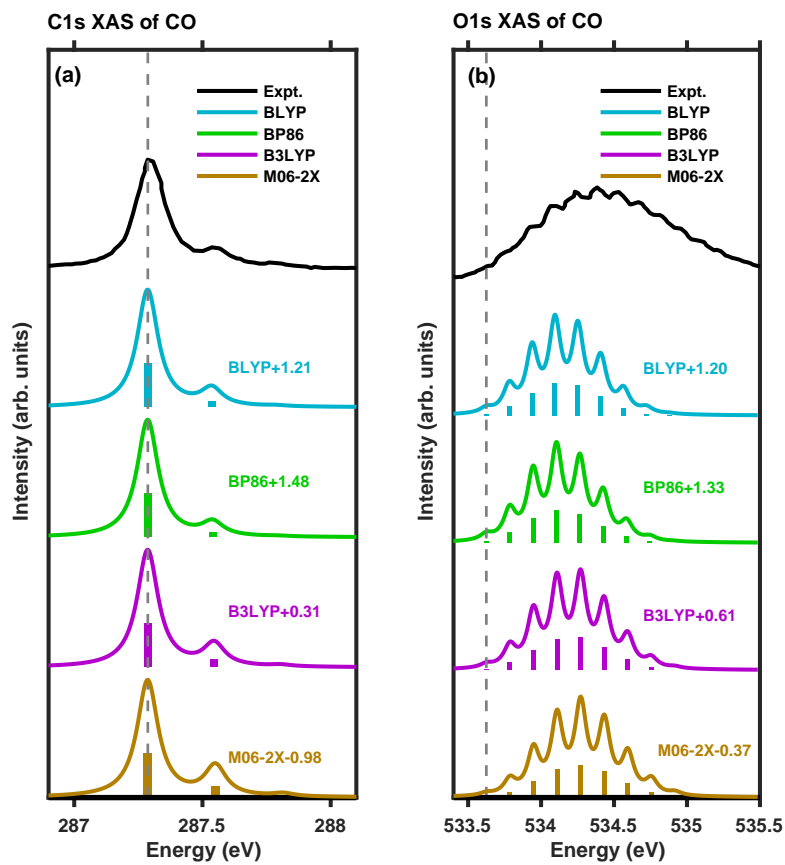


Figure 4: The same as Fig. 2 for simulated vibrationaly-resolved XAS of CO: (a) C1s and (b) O1s edges. The experiment for comparison was taken from Hitchcock et al.[61] and Püttner et al.[28]

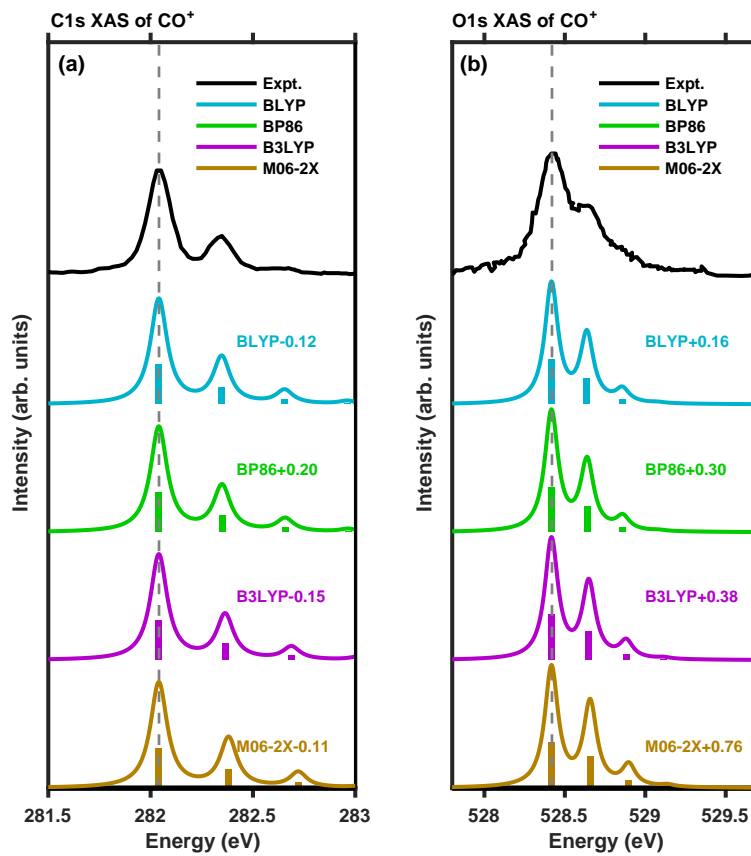


Figure 5: The same as Fig. 2 for simulated vibrationaly-resolved XAS spectra of CO^+ : (a) C1s and (b) O1s edges. The experiment was taken from Couto et al.[31]

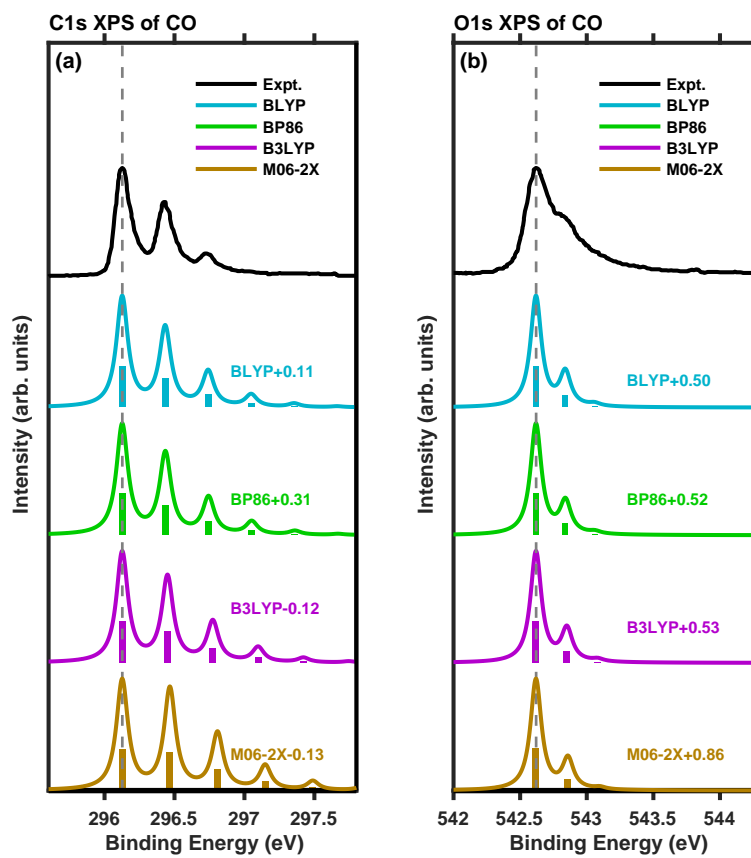


Figure 6: The same as Fig. 2 for simulated vibrationaly-resolved XPS spectra of CO: (a) C1s and (b) O1s edges. The experiment was taken from Hergenahn.[2]